Evaluating Performances of Simplified Physically Based Models for Landslide Susceptibility.

Giuseppe Formetta, Giovanna Capparelli and Pasquale Versace

University of Calabria Dipartimento di Ingegneria Informatica, Modellistica, Elettronica e Sistemistica Ponte Pietro Bucci, cubo 41/b, 87036 Rende, Italy (giuseppe.formetta@unical.it, giovanna.capparelli@unical.it, pasquale.versace@unical.it)

Abstract: Rainfall induced shallow landslides cause loss of life and significant damages involving private and public properties, transportation system, etc. Prediction of shallow landslides susceptible locations is a complex task that involves many disciplines: hydrology, geotechnical science, geology, hydrogeology, geomorphology, and statistics. Usually to accomplish this task two main approaches are used: statistical or physically based model. Reliable models' applications involve: automatic parameters calibration, objective quantification of the quality of susceptibility maps, model sensitivity analysis. This paper presents a methodology to systemically and objectively calibrate, verify and compare different models and different models performances indicators in order to individuate and eventually select the models whose behaviors are more reliable for a certain case study.

The procedure was implemented in package of models for landslide susceptibility analysis and integrated in the NewAge-JGrass hydrological model. The package includes three simplified physically based models for landslides susceptibility analysis (M1, M2, and M3) and a component for models verifications. It computes eight goodness of fit indices by comparing pixel-by-pixel model results and measurements data. Moreover, the package integration in NewAge-JGrass allows the use of other components such as geographic information system tools to manage inputs-output processes, and automatic calibration algorithms to estimate model parameters.

The system was applied for a case study in Calabria (Italy) along the Salerno-Reggio Calabria highway, between Cosenza and Altilia municipality. The analysis provided that among all the optimized indices and all the three models, the optimization of the index distance to perfect classification in the receiver operating characteristic plane (D2PC) coupled with model M3 is the best modeling solution for our test case.

***Keywords**:* Landslide modelling; Object Modeling System; Models calibration.

1 INTRODUCTION

Landslides are one of major worldwide dangerous geo-hazards and constitute a serious menace the public safety causing human and economic loss (Park 2011). Geo-environmental factors such as geology, land-use, vegetation, climate, increasing population may increase the landslides occurrence (Sidle and Ochiai 2006). Landslide susceptibility assessment, i.e. the likelihood of a landslide occurring in an area on the basis of local terrain conditions (Brabb, 1984), is not only a crucial aspect for an accurate landslide hazard quantification but also a fundamental tool for the environment preservation and a responsible urban planning (Cascini et al., 2005).

During the last few decades many methods for landslide susceptibility mapping were developed and they can be grouped in two main branches: qualitative and quantitative methods (Glade and Crozier, 2005, Corominas et al., 2014 and references therein).

Qualitative methods, based on field campaigns and on the basis of expert knowledge and experience, are subjective but necessary to validate quantitative methods results. Quantitative methods include statistical and physically based methods. Statistical methods (e.g. Naranjo et al., 1994, Chung et al. 1995, Guzzetti et al., 1999, Catani et al., 2005) use different approaches such as multivariate analysis, discriminant analysis, random forest to link instability factors (such as geology, soils, slope, curvature, and aspect) with the past and present landslides.

Deterministic models (e.g. Montgomery and Dietrich, 1994, Lu and Godt, 2008, Borga et al., 2002, Simoni et al., 2008, Capparelli and Versace, 2011, Lu and Godt, 2013) synthetize the interaction between hydrology, geomorphology, and soil mechanics in order to physically understand and predict landslides triggering location and timing. In general, they include a hydrological and a slope stability component.

The hydrological component simulates infiltration and groundwater flow processes with different degree of simplification, from steady state (e.g. Montgomery and Dietrich, 1994) to transient analysis (Simoni et al., 2008). The soil-stability component simulates the slope safety factor (FS) defined as ratio of stabilizing to destabilizing forces.

Results of a landslide susceptibility analysis strongly depend on the model hypothesis, parameters values, and parameters estimation method. Problems such as the evaluation landslide susceptibility model performance, the choice of the best accurate model, and the selection of the most performing method for parameter estimation are still opened. For these reasons, a procedure that allows objective comparisons between different models and evaluation criteria aimed to the selection of the most accurate models is needed.

Many efforts were devoted to the crucial problem of evaluating landslide susceptibility models performances (e.g Dietrich et al., (2001), Frattini et al., (2010) and Guzzetti et al., (2006)). Accurate discussions about the most common quantitative measures of goodness of fit (GOF) between measured and modeled data are available in Bennet et al., (2013), Jolliffe and Stephenson, (2012), Beguería (2006), Brenning (2005) and references therein. We summarized them in Appendix 1. Wrong classifications in landslide susceptibility analysis involve not only risk of loss of life but also economic consequences. For example locations classified as stable increase their economical value because no construction restriction will be applied, and vice-versa for locations classified as unstable.

In this work we propose an objective methodology for environmental models analysis that allows to select the most performing model based on a quantitative comparison and assessment of models prediction skills. In this paper the methodology is applied for assessing the performances of simplified landslide susceptibility models. Moreover, being the methodology model independent, it can be used for assessing the ability of any type of environmental model to simulate natural phenomena. The procedure is implemented in the open source and GIS based hydrological model, denoted as NewAge-JGrass (Formetta et al., 2014) that uses the Object Modeling System (OMS, David et al., 2013) modeling framework.

OMS is a Java based modeling framework that promotes the idea of programming by components and provides the model developers with many facilitates such as: multithreading, implicit parallelism, models interconnection, and GIS based system.

The NewAge-JGrass system, fig. 1, contains models, automatic calibration algorithms for model parameters estimation, and methods for estimating the goodness of the models prediction. The open source GIS uDig (http://udig.refractions.net/) and the uDig-Spatial Toolbox (Abera et al., (2014), https://code.google.com/p/jgrasstools/wiki/JGrassTools4udig) are used as visualization and input/out data management system.

The methodology for landslide susceptibility analysis (LSA) represents one model configuration into the more general NewAge-JGrass system. It includes two new models specifically developed for this paper: mathematical components for landslide susceptibility mapping and procedures for landslides susceptibility model verification selection. Moreover LSA configuration uses two models already implemented in NewAge-JGrass: the geomorphological model set-up and the automatic calibration algorithms for model parameter estimation. All the models used in the LSA configuration are presented in Fig. 1, encircled dashed red line.

For a generic landslide susceptibility component it is possible to estimate the model parameters that optimize a given GOF metric. To perform this step the user can choose between a set of GOF indices and a set of automatic calibration algorithms. Comparing the results obtained for different models and for deferent GOF metrics the user can select the most performing combination for his or her own case study

The methodology, accurately presented in section 2, was setup considering three different landslide susceptibility models, eight GOF metrics, and one automatic calibration algorithm. The flexibility of the system allows to add more models, GOF metrics, and to use different calibration algorithms. Thus deferent LSA configurations can be realized depending on: the landslide susceptibility model, the calibration algorithm, and the GOFs selected by the user.

Lastly, section 3 presents a case study of landslide susceptibility mapping along the A3 Salerno-Reggio Calabria highway in Calabria, that illustrates the capability of the system.

2 MODELING FRAMEWORK

The landslide susceptibility analysis (LSA) is implemented in the context of NewAge-JGrass (Formetta et al., 2014), an open source large-scale hydrological modeling system. It models the whole hydrological cycle: water balance, energy balance, snow melting, etc. (Figure 1). The system implements hydrological models, automatic calibration algorithms for model parameter optimization, and evaluation, and a GIS for input output visualization, (Formetta et al., 2011, Formetta et al., 2014). NewAge-JGrass is a component-based model: each hydrological process is described by a model (energy balance, evapotranspiration, run off production in figure 1); each model implement one or more component(s) (considering for example the model evapotranspiration in figure 1, the user can select between three different components: Penman-Monteith, Priestly-Taylor, and Fao); each component can be linked to the others and executed at runtime, building a model configuration. Figure 1 offers a complete picture of the system and the integration of the new LSA configuration encircled dashed red line. More precisely the LSA in the actual configuration includes two new models: a landslides susceptibility model and a model for model verification and selection. The first includes three components proposed in Montgomery and Dietrich, 1994, Park et al., 2013, and Rosso et al., 2006, the latter includes the “Three steps verification procedure” (3SVP), accurately presented in section 2. Moreover LSA configuration includes other two models beforehand implemented in the NewAge-JGrass system: i) the Horton Machine for geomorphological model setup that compute input maps such as slope, total contributing area and visualize model results, and ii) the Particle Swarm for automatic calibration. Subsection 2.1 presents the landslide susceptibility model and subsection 2.2 the model selection procedure (3SVP).

2.1 Landslide susceptibility models

The landslide susceptibility models implemented in NewAge-JGrass and presented in a preliminary application in Formetta et al., 2015 are: the Montgomery and Dietrich (1994) model (M1), the Park et al. (2013) model (M2) and the Rosso et al. (2006) model (M3). The tree models derives from simplifications of the infinite slope equation (Grahm J., 1984, Rosso et al., 2006, Formetta et al., 2014) for the factor of safety:

$$FS = \frac{C\cdot(1+e)}{\left[G_s + e\cdot S_r + w\cdot e\cdot\left(1-S_r\right)\right]\cdot\gamma_w\cdot H\cdot\sin\alpha\cdot\cos\alpha} + \frac{\left[G_s + e\cdot S_r - w\cdot\left(1+e\cdot S_r\right)\right]}{\left[G_s + e\cdot S_r + w\cdot e\cdot\left(1-S_r\right)\right]}\cdot\frac{\tan\varphi'}{\tan\alpha} \quad (1)$$

where FS [-] is the factor of safety, $C=C'+C_{root}$ is the sum of C_{root}, the root strength [kN/m2] and C' the effective soil cohesion [kN/m2], φ' [-] is the internal soil friction angle, H is the soil depth [m], α [-] is the slope angle, γ_w [kN/m3] is the specific weight of water, and w=h/H [-] where h [m] is the water table height above the failure surface [m], Gs [-] is the specific gravity of soil, e [-] is the average void ratio and Sr [-] is the average degree of saturation.

The model M1 assumes hydrological steady-state, flow occurring in the direction parallel to the slope and neglect, cohesion, degree of soil saturation and void ratio. It computes w as:

$$w = \frac{h}{H} = \min\left(\frac{Q}{T}\cdot\frac{TCA}{b\cdot\sin\alpha}, 1.0\right) \quad (2)$$

where T [L^2/T] is the soil transmissivity defined as the product of the soil depth and the saturated hydraulic conductivity, b [L] is the length of the contour line. Substituting eq. (2) in (1) the model is solved for Q/T assuming FS=1 and stable and unstable sites are defined using threshold values on log(Q/T) (Montgomery and Dietrich, 1994).

Differently from M1, the model M2 considers: i) the effect of the degree of soil saturation (S_r [-]) and void ratio (e [-]) above the groundwater table and ii) the stabilizing contribute of the soil cohesion. The model output is a map of safety factors (FS) for each pixel of the analyzed area.

The component (M3) considers both the effects of rainfall intensity and duration on the landslide triggering process. The term w depends on rainfall duration and it is obtained by coupling the conservation of mass of soil water with the Darcy's law (Rosso et al., 2006) providing:

$$w=\begin{cases} \dfrac{Q}{T}\cdot\dfrac{TCA}{b\cdot\sin\alpha}\cdot\left[1-\exp\left(\dfrac{e+1}{e\cdot(1-S_r)}\cdot\dfrac{t}{T}\cdot\dfrac{TCA}{b\cdot\sin\alpha}\cdot H\right)\right] & \text{if } \dfrac{t}{T}\cdot\dfrac{TCA}{b\cdot\sin\alpha}\cdot H\le-\dfrac{e\cdot(1-S_r)}{1+e}\cdot\ln\left(1-\dfrac{T\cdot b\cdot\sin\alpha}{TCA\cdot Q}\right) \\ 1 & \text{if } \dfrac{t}{T}\cdot\dfrac{TCA}{b\cdot\sin\alpha}\cdot H>-\dfrac{e\cdot(1-S_r)}{1+e}\cdot\ln\left(1-\dfrac{T\cdot b\cdot\sin\alpha}{TCA\cdot Q}\right) \end{cases} \quad (3)$$

Those models are suitable for shallow translational landslides controlled by groundwater flow convergence. Shallow landslides usually have a very low ratio between the maximum depth (D) and the length (L) of scar (D/L<0.1, Casadei et al., 2003), involve small volume of the colluvial soil mantle and present a generally translational failure mechanism (Milledge et al., 2014).

Each component has a user interface which specifies input and output. Model input are computed in the GIS uDig integrated in the NewAge-JGrass system by using the Horton Machine package for terrain analysis (Abera et al., 2014). Model output maps are directly imported in the GIS and available for user's visualization.

The models that we implemented present increasing degree of complexity on the theoretical assumptions for modeling landslide susceptibility. Moving from M1 to M2 soil cohesion and soil properties were considered, and moving from M2 to M3 rainfall of finite duration was used.

2.2 Automatic calibration and model verification procedure

In order to assess the models' performance we developed a model that computes the most used indices for assessing the quality of a landslide susceptibility map.

These are based on pixel-by-pixel comparison between observed landslide map (OL) and predicted landslides (PL). They are binary maps with positive pixels corresponding to "unstable" ones, and negative pixels that correspond to "stable" ones. Therefore, four types of outcomes are possible for each cell. A pixel is a true-positive (tp) if it is mapped as "unstable" both in OL and in PL, that is a correct alarm with well predicted landslide. A pixel is a true-negative (tn) if it is mapped as "stable" both in OL in PL, that correspond to a well predicted stable area. A pixel is a false-positive (fp) if it is mapped as "unstable" in PL, but is "stable" in OL; that is a false alarm. A pixel is a false-negative (fn) if it is mapped as "stable" in PL, butt is "unstable" in OL, that is a missed alarm. The concept of the Receiver Operator

Characteristic (ROC, Goodenough et al., 1974) graph is based on the values assumed by tp, fp, tn. The ROC is a methodology to assess the performance of models that provides results assigned to one of two classes. ROC graph is widely used in many scientific fields such as medicine (Goodenough et al., 1974), biometrics (Pepe, 2003) and machine learning (Provost and Fawcett, 2001). ROC graph is a Cartesian plane with the FPR on the x-axis and TPR on the y-axis. FPR is the ratio between false positive and the sum of false positive and true negative, and TPR is the ratio between true positive and the sum of true positive and false negative. They are defined in table 1 and commented in Appendix 1. The performance of a perfect model corresponds to the point P(0,1) on the ROC plane; points that fall on the bisector (black solid line, on the plots) are associated with models considered random: they predict stable or unstable cells with the same rate.

Eight GOF indices for quantification of model performances are implemented in the system. Table (1) shows their definition, range, and optimal values. A more accurate description of the indices is provided in Appendix 1.

Automatic calibration algorithms implemented in NewAge-JGrass as OMS components can be used in order to tune model parameters for reproducing the actual landslide. This is possible because each model is an OMS component and can be linked to the calibration algorithms as it is, without rewriting or modifying its code. Three calibration algorithms are embedded in the system core: Luca (Hay et al., 2006), a step-wise algorithm based on shuffle complex evolution (Duan et al., 1992), Particle Swarm Optimization (PSO), a genetic model presented in (Kennedy and Eberhart, 1995), and DREAM (Vrugt et al., 2008) acronym of Differential Evolution Adaptive Metropolis. In actual configuration we used Particle Swarm Optimization (PSO) algorithm to estimate model parameters optimal values.

During the calibration procedure the selected algorithm compares model output in term of binary map (stable or unstable pixel) with the actual landslide optimizing a selected objective function (OF). The model parameter set for which the OF assumes its best value is the optimization procedure output. The eight GOF indices presented in table 1 were used in turn as OF and, consequently, eight optimal parameters sets were provided as calibration output (one for each optimised OF). To better clarify: a GOF index selected in table 1 becomes an OF when it is used as objective function of the automatic calibration algorithm.

In order to quantitatively analyze the model performances we implemented a three steps verification procedure (3SVP). Firstly we evaluated the performances of every single OF index for each model. We presented the results in the ROC plane in order to asses what is (are) the OF index(es) whose optimization provides best model performances. Secondly, we verified if each OF metric has its own information content or if it provides information analogous to other metrics (and unessential).
Lastly, for each model, the sensitivity of each optimal parameter set is tested by perturbing optimal parameters and by evaluating their effects on the GOF.

3 MODELING FRAMEWORK APPLICATION

The LSA presented in the paper is applied for the highway Salerno-Reggio Calabria in Calabria region (Italy), between Cosenza and Altilia. Subsection 3.1 describes the test-site; subsection 3.2 describes the model parameters calibration and verification procedure; subsection 3.3 presents the models performances correlations assessment; lastly, subsection 3.4 presents the robustness analysis of the GOF indices used.

3.1 Site Description

The test site was located in Calabria, Italy, along the Salerno-Reggio Calabria highway between Cosenza and Altilia municipalities, in the southern portion of the Crati basin (Figure 2). The mean annual precipitation is about of 1200 mm, distributed on about 100 rainy days, and mean annual temperature of 16 °C. Rainfall peaks occur in the period October–March, during which mass wasting and severe water erosion processes are triggered (Capparelli et al., 2012, Conforti et al., 2011, Iovine et al., 2010).
In the study area the topographic elevation has an average value of around 450 m a.s.l., with a maximum value of 730 m a.s.l. Slope, computed from 10 meters

resolution digital elevation model, range from 0° to 55°, while its average is about 26°.

The Crati Basin is a Pleistocene-Holocene extensional basin filled by clastic marine and fluvial deposits (Vezzani, 1968, Colella et al., 1987, Fabbricatore et al., 2014). The stratigraphic succession of the Crati Basin can be simply divided into two sedimentary units as suggested by Lanzafame and Tortorici, 1986. The first unit is a Lower Pliocene succession of conglomerates and sandstones passing upward into silty clays (Lanzafame and Tortorici, 1986) second unit. This is a succession of clayey deposits grading upward into sandstones and conglomerates referred to Emilian and Sicilian, respectively (Lanzafame and Tortorici, 1986), as also suggested by data provided by Young and Colella (1988). Mass movements were analyzed from 2006 to 2013 by integrating aerial photography interpretation acquired in 2006, 1:5000 scale topographic maps analysis, and extensive field survey.

All the data were digitized and stored in GIS database (Conforti et al., 2014) and the result was the map of occurred landslide presented in figure 2,D. Digital elevation model, slope and total contributing area (TCA) maps are presented in figure 2, A, B, and C respectively. In order to perform model calibration and verification, the dataset of occurred landslides was divided in two parts one used for calibration (located in the bottom part of figure 2,D) and one for validation (located in the upper part of the figure 2,D). The landslide inventory map refers only to the initiation area of the landslides. This allows a fair comparison with the landslide models that provide only the triggering point and not include a runout model for landslides propagation.

3.2 Models calibration and verification

The three models presented in section 2 were applied to predict landslide susceptibility for the study area. Models' parameters were optimized using each GOF index presented in table 1 in order to fit landslides of the calibration group. Table 2 presents the list of the parameters that will be optimized specifying their initial range of variation, and the parameters kept constant during the simulation and their value.

The component PSO provides 8 best parameters set one for each optimized GOF indices. Values for each model (M1, M2 and M3) were presented in table 3. Optimal parameter sets are slightly different among the models and among the optimized GOF indices for a fixed model. Moreover a compensation effect between parameter values is evident: high values of friction angles are related to low cohesion values or high values of critical rainfall are related to high values of soil resistance parameters. Considering the model M1, transmissivity value (74 m2/d) optimizing ACC is much lower compared to the transmissivity values obtained optimizing the other index (around 140 m2/d). Similar behavior is observed for the optimal rainfall value which is 148 [mm/d] optimizing ACC and around 70 [mm/d] optimizing the other indices. Considering the model M2, the optimal transmissivity and rainfall values optimizing CSI (10 [m2/d] and 95 [mm/d]), are much lower compared the values obtained optimizing the other indices (around 50 [m2/d] and 250 [mm/d] in average). For the model M3, instead, optimal parameters present the same order of magnitude for all optimized indices. This suggests that the variability of the optimal parameter values for models M1 and M2 could be due to compensate the effects of important physical processes neglected by those models.

Executing the models using the eight optimal parameters set, true-positive-rates and false positive rates are computed by comparing model output and actual landslides for both calibration and verification dataset. Results are presented in Table 4, for all three models M1, M2 and M3. Those points were reported in the ROC plane in order to visualize in a unique graph the effects of the optimised objective function on model performances. This procedure was repeated for the three models. ROC planes considering all the GOF indices and all three models are included in Appendix 2 both for calibration and for verification period. For the models M2 and M3 is clear that ACC, HSS, and CSI provide the less performing models results. This is true also for model M1, even if, differently form M2 and M3, there is not a so clear separation between the performances provided by ACC, HSS, and CSI and the remaining indices.

Among the results provided in Table 4, we focused our attention only on the GOF indices whose optimization satisfies the condition: FPR<0.4 and TPR>0.7. This choice was made in order to restrict the results' comments only on the GOF indices that provide acceptable model results and for the readability of graphs.

Figure 3 presents three ROC planes, one for each model, with the optimized GOF indices that provides FPR<0.4 and TPR>0.7. Results presented in Figure 3 and

Table 4 show that: i) optimization of AI, D2PC, SI and TSS allows to reach the best model performance in the ROC plane, and this is verified for all three models; ii) performances increase as model complexity increases: moving from M1 to M3 points in the ROC plane approaches the perfect point (TPR=1, FPR=0); iii) increasing model complexity good model results are reached not only in calibration but also in validation dataset. In fact, moving from M1 to M2 soil cohesion and soil properties were considered, and moving from M2 to M3 rainfall of finite duration was used.
The first step of the 3SVP procedure remarks that the optimization of AI, D2PC, SI, and TSS provides the best performances independently of the model we used.

3.3 Models performances correlations assessment

The secondo step of the procedure aims to verify the information content of each optimized OF, checking if it is analogous to other metrics or it is peculiar of the optimized OF.
Executing a model using one of the eight parameters set (let's assume, for example, the one obtained optimizing CSI) allows the computation of all the remaining GOF indices, that we indicate as CSI_{CSI}, ACC_{CSI}, HSS_{CSI}, TSS_{CSI}, AI_{CSI}, SI_{CSI}, $D2PC_{CSI}$, ESI_{CSI}, both for calibration and for verification dataset. Let's denote this vector with the name $\boldsymbol{MP_{CSI}}$: the model performances (***MP***) vector computed using the parameters set that optimize CSI. $\boldsymbol{MP_{CSI}}$ has 16 elements, 8 for calibration and 8 for validation dataset. Repeating the same procedure for all eight GOF indices it gives: $\boldsymbol{MP_{ACC}}$, $\boldsymbol{MP_{ESI}}$, $\boldsymbol{MP_{SI}}$, $\boldsymbol{MP_{D2PC}}$, $\boldsymbol{MP_{TSS}}$, $\boldsymbol{MP_{AI}}$, $\boldsymbol{MP_{HS}}$. Figure 4 presents the correlation plots (Murdoch and Chow, 1996) between all ***MP*** vectors, for each model M1, M2 or M3. The matrix is symmetric and gives a certain ellipse at intersection of row i and column j. The color is the absolute value of the correlation coefficient between the $\boldsymbol{MP_i}$ and $\boldsymbol{MP_j}$ vectors. The ellipse's eccentricity is scaled according to the correlation value: the more prominent the less the vectors are correlated; if ellipse leans towards the right correlation is positive and if it leans to the left, it is negative.
All indices present a positive correlation among each other independent of the model used. Moreover strong correlations between the ***MP*** vectors of AI, D2PC, SI and TSS are evident in figure 4. This confirms that an optimization of AI, D2PC, SI and TSS provides quite similar model performances, and this is independent of the

model used. On the other hand the remaining GOF indices give quite different information from the previous four indices, but they gave worse performances in first step analysis. Thus in the case study using one of the four best GOF can be enough for parameter estimation.

3.4 Models sensitivity assessment

In this step we focused on the models M2 and M3 and we performed a parameter sensitivity analysis. Let's assume to consider model M2 and the optimal parameter set computed by optimizing the Critical Success Index (CSI). Moreover let's assume to consider the cohesion model parameter, the procedure evolves according the following steps:

- The starting parameter values are the optimal values derived from the optimization of the CSI index;
- All the parameters except the analyzed parameter (cohesion) were kept constant and equal to the optimal parameter set;
- 1000 random values of the analyzed parameter (cohesion) were picked up from a uniform distribution with lower and upper bound defined in Table 1. With this procedure 1000 model parameter sets were defined and used to execute the model.
- 1000 values of the selected GOF index (CSI), computed by comparing model outputs with measured data, were used to compute a boxplot of the parameter C and optimized index CSI.

The procedure was repeated for each parameter and for each optimized index. Results were presented in Figures 5 and 6 for models M2 and M3 respectively.

Each column of the figures represents one optimized index and has a number of boxplots equal to the number of model's parameters (5 for M2 and 6 for M3). Each boxplot represents the range of variation of the optimized index due to a certain model parameters change. The narrower the boxplot for a given optimized index the less sensitive is the model to that parameter. For both M2 and M3 the parameter set obtained by optimizing AI and SI shows the less sensitive behavior for almost all parameters. In this case a model parameter perturbation does not influence much the model performances. On the contrary, the models whit parameters obtained by optimizing ACC, TSS, and D2PC are the more sensitive to the parameters variations and this is reflected in much more evident changing of model performances.

3.5 Models selections and susceptibility maps

The selection of the more appropriate model for computing landslide susceptibility maps is based on what we learn from the previous steps. In the first step we learn that i) optimization of AI, D2PC, SI and TSS outperform the remaining indices and ii) models M2 and M3 provides more accurate results compared to M1. The second step suggests that overall models results obtained by optimizing AI, D2PC, SI and TSS are similar each other. Lastly, the third step shows that models performance derived from the optimization of AI and SI are the less sensible to input variations compared to D2PC and TSS. This behavior could be due the formulation of AI and SI that gives much more weight to the true negative compared to D2PC and TSS.

In particular for our application, the model M3 whit parameters obtained by optimizing D2PC was the most sensitive to the parameter variation avoiding an “insensitive” or flat response changing the parameters value. A more sensitive couple model-optimal parameter set will in fact accommodate eventual parameters, input data, or measured data variations responding to these changes with a variation of model performance.

For this reason we used the combination the model M3 with parameters obtained by optimizing D2PC for drawing the final susceptibility maps in figure 7. Categories of landslides susceptibility from class 1 to 5 are assigned from low to high according to FS values (e.g. Huang et al., 2007): Class 1 ($FS<1.0$), Class 2 ($1.0<FS<1.2$), Class 3 ($1.2<FS<1.5$), Class 4 ($1.5<FS<2.0$), Class 5 ($FS>2$).

4 Conclusions

The paper presents a procedure to quantitatively calibrate, evaluate, and compare the performances of environmental models. The procedure was applied for the analysis of three landslides susceptibility models. It includes 3 steps: i) model parameters calibration optimizing different GOF indices and models evaluation in the ROC plane; ii) computation of degree of similarities between different models performances obtained by optimizing all the considered GOF index; iii) evaluation of models sensitivity to parameters variations.

The procedure has been conceived like a model configuration of the hydrological system NewAge-JGrass; it integrates: i) three simplified physically based landslides susceptibility models; ii) a package for model evaluations based on pixel-by-pixel comparison of modeled and actual landslides maps; iii) models parameters calibration algorithms, and iv) the integration with uDig open-source geographic information system for model input-output maps management.

This procedure was applied in a test case on the Salerno-Reggio Calabria highway and the best model performances were provided by model M3 optimizing D2PC index. In the application we presented the effective precipitation was calibrated because we were performing a landslide susceptibility analysis and it was useful for demonstrating the method. However, we are aware that for operational landslide early warning systems the rainfall constitutes a fundamental input of the predictive process. Moreover, the analysis would profit from measured rainfall data that triggered the occurred landslides, but that such data are not available at the moment for the study area.

The system is open-source and available at (https://github.com/formeppe). It is integrated according the Object Modeling System standards and this allows the user to easily integrate a generic landslide susceptibility model and use the complete framework presented in the paper avoiding rewriting programming code. The system will be helpful for decision makers that deal with risk management assessment and could be improved by adding new landslide susceptibility models or different types of model selection procedure.

ACKNOWLEDGMENTS

This research was funded by PON Project No. 01_01503 “Integrated Systems for Hydrogeological Risk Monitoring, Early Warning and Mitigation Along the Main Lifelines”, CUP B31H11000370005, in the framework of the National Operational Program for "Research and Competitiveness" 2007-2013. The authors acknowledge the editor and the three reviewers (Prof. M. Mergili and two unknown reviewers) for providing insightful comments and improving the quality of the paper.

Acronyms table

3SVP	Three steps verification procedure
AI	Average Index
CSI	Critical success index
D2PC	Distance to perfect classification
ESI	Equitable success index
fn	False negative
fp	False positive
FPR	False positive rate
FS	Factor of safety
GIS	Geographic informatic system
GOF	Goodness of fit indices
HSS	Heidke skill score
LSA	Landslide susceptibility analysis
M1	Model for landslide susceptibility analysis proposed in Montgomery and Dietrich, 1994
M2	Model for landslide susceptibility analysis proposed in Park et al., 2013
M3	Model for landslide susceptibility analysis proposed in Rosso et al., 2006
MP	Model performances vector
OF	Objective function
OL	Observed landslide map
OMS	Object modeling system
PL	Predicted landslide map
PSO	Particle Swarm optimization
ROC	Receiver operating characteristic
SI	Success index
TCA	Total contributing area
tn	True negative
tp	True positive
TPR	True positive rate
TSS	True Skill Statistic

REFERENCES

Abera W., A. Antonello, S. Franceschi, G. Formetta, R Rigon , "The uDig Spatial Toolbox for hydro-geomorphic analysis" in GEOMORPHOLOGICAL TECHNIQUES, v. 4, n. 1 (2014), p. 1-19. - URL: http://www.geomorphology.org.uk/sites/default/files/geom_tech_chapters/2.4.1_GISToolbox.pdf

Beguería, S. (2006). Validation and evaluation of predictive models in hazard assessment and risk management. *Natural Hazards*, *37*(3), 315-329.

Bennett ND, Croke BF, Guariso G, Guillaume JH, Hamilton SH, Jakeman AJ, Marsili-Libelli S, Newham LT, Norton JP, Perrin C, Pierce SA. Characterising performance of environmental models. Environmental Modelling & Software. 2013 Feb 28;40:1-20.

Borga, M., Dalla Fontana, G., & Cazorzi, F. (2002). Analysis of topographic and climatic control on rainfall-triggered shallow landsliding using a quasi-dynamic wetness index. Journal of Hydrology, 268(1), 56-71.

Brabb, E.E., (1984). Innovative approaches to landslide hazard and risk mapping, Proceedings of the 4th International Symposium on Landslides, 16–21 September, Toronto, Ontario, Canada (Canadian Geotechnical Society, Toronto, Ontario, Canada), 1:307–324

Brenning, A. "Spatial prediction models for landslide hazards: review, comparison and evaluation." *Natural Hazards and Earth System Science* 5, no. 6 (2005): 853-862.

Capparelli, G., & Versace, P. (2011). FLaIR and SUSHI: two mathematical models for early warning of landslides induced by rainfall. Landslides, 8(1), 67-79.

Capparelli G, Iaquinta P, Iovine GGR, Terranova OG, Versace P. Modelling the rainfall-induced mobilization of a large slope movement in northern Calabria. Natural Hazards 2012 ;61:247–256.

Casadei, M., Dietrich, W. E., & Miller, N. L. (2003). Testing a model for predicting the timing and location of shallow landslide initiation in soil‐mantled landscapes. *Earth Surface Processes and Landforms*, *28*(9), 925-950.

Cascini, L., Bonnard, C., Corominas, J., Jibson, R., & Montero-Olarte, J. (2005). Landslide hazard and risk zoning for urban planning and development. *Landslide Risk Management. Taylor and Francis, London*, 199-235.

Catani, F., Casagli, N., Ermini, L., Righini, G., & Menduni, G. (2005). Landslide hazard and risk mapping at catchment scale in the Arno River basin. *Landslides*, *2*(4), 329-342.

Chung C-JF, Fabbri AG and van Westen CJ (1995) Multivariate regression analysis for landslide hazard zonation. Carrara A and Guzzetti F (Eds.) Geographical Information Systems in assessing natural hazards. Dordrecht, Kluwer Academic Publishers. 5:107-34

Colella A, De Boer PL, Nio SD. Sedimentology of a marine intermontane Pleistocene Gilbert-type fan-delta complex in the Crati Basin, Calabria, southern Italy. Sedimentology 1987;34:721–736.

Conforti, M., Pascale, S., Robustelli, G., & Sdao, F. (2014). Evaluation of prediction capability of the artificial neural networks for mapping landslide susceptibility in the Turbolo River catchment (northern Calabria, Italy). Catena, 113, 236-250.

Conforti M, Aucelli PPC, Robustelli G, Scarciglia F. Geomorphology and GIS analysis for mapping gully erosion susceptibility in the Turbolo Stream catchment (Northern Calabria, Italy). Natural Hazards 2011;56:881–898.

Corominas J, Van Westen C, Frattini P, Cascini L, Malet JP, Fotopoulou S, Catani F, Van Den Eeckhaut M, Mavrouli O, Agliardi F, Pitilakis K. Recommendations for the quantitative analysis of landslide risk. Bulletin of engineering geology and the environment. 2014 May 1;73(2):209-63.

Dietrich, W. E., Bellugi, D. and Real De Asua, R. (2001) Validation of the Shallow Landslide Model, SHALSTAB, for Forest Management, in Land Use and Watersheds: Human Influence on Hydrology and Geomorphology in Urban and Forest Areas (eds M. S. Wigmosta and S. J. Burges), American Geophysical Union, Washington, D. C.. doi: 10.1029/WS002p0195

David, O., Ascough II, J. C., Lloyd, W., Green, T. R., Rojas, K. W., Leavesley, G. H., & Ahuja, L. R. (2013). A software engineering perspective on environmental modeling framework design: The Object Modeling System. Environmental Modelling & Software, 39, 201-213.

Duan, Q., Sorooshian S., and Gupta V(1992): Effective and efficient global optimization for conceptual rainfall-runoff models. Water Resources Research 28.4 (1992): 1015-1031.

Duncan, J. M., and S. G. Wright (2005), Soil Strength and Slope Stability, 297 pp., New Jersey, John Wiley.

Fabbricatore D, Robustelli G, Muto F. Facies analysis and depositional architecture of shelf-type deltas in the Crati Basin (Calabrian Arc, south Italy). Boll. Soc. Geol. It. 2014;133(1):131-148.

Formetta, G., Mantilla, R., Franceschi, S., Antonello, A., & Rigon, R. (2011). The JGrass-NewAge system for forecasting and managing the hydrological budgets at the basin scale: models of flow generation and propagation/routing. Geoscientific Model Development, 4(4), 943-955.

Formetta, G., Antonello, A., Franceschi, S., David, O., & Rigon, R. (2014). Hydrological modelling with components: A GIS-based open-source framework. Environmental Modelling & Software, 55, 190-200.

Formetta, G., Capparelli, G., Rigon, R., and Versace, P.: Physically based landslide susceptibility models with different degree of complexity: calibration and verification. International Environmental Modelling and Software Society (iEMSs). 7th Intl. Congress on Env. Modelling and Software, San Diego, CA, June 15-19, USA, Daniel P. Ames, Nigel W.T. Quinn and Andrea E. Rizzoli (Eds.), 2014. http://www.iemss.org/sites/iemss2014/papers/iemss2014_submission_157.pdf

Frattini, P., Crosta, G., & Carrara, A. (2010). Techniques for evaluating the performance of landslide susceptibility models. Engineering geology, 111(1), 62-72.

Guzzetti, Fausto, Alberto Carrara, Mauro Cardinali, and Paola Reichenbach. "Landslide hazard evaluation: a review of current techniques and their application in a multi-scale study, Central Italy." *Geomorphology* 31, no. 1 (1999): 181-216.

Guzzetti, F., Reichenbach, P., Ardizzone, F., Cardinali, M., & Galli, M. (2006). Estimating the quality of landslide susceptibility models. Geomorphology, 81(1), 166-184.

Glade, T., & Crozier, M. J. (2005). A review of scale dependency in landslide hazard and risk analysis. Landslide hazard and risk, Vol. 3, 75-138.

Goodenough, D.J., Rossmann, K., Lusted, L.B., 1974. Radiographic applications of receiver operating characteristic (ROC) analysis. Radiology 110, 89–95.

Grahm J (1984) Methods of slope stability analysis. In: Brunsden D, Prior DB (eds) Slope instability. Wiley, New York, pp 171–215

Hay, L.E., G.H. Leavesley, M.P. Clark, S.L. Markstrom, R.J. Viger, and M. Umemoto (2006). Step-Wise, Multiple-Objective Calibration of a Hydrologic Model for a Snowmelt-Dominated Basin. Journal of the American Water Resources Association 42:877-890, 2006

Huang, J. C., Kao, S. J., Hsu, M. L., & Liu, Y. A. (2007). Influence of Specific Contributing Area algorithms on slope failure prediction in landslide modeling. *Natural Hazards and Earth System Science*, *7*(6), 781-792.

Lanzafame G, Tortorici L. La tettonica recente del Fiume Crati (Calabria). Geografia Fisica e Dinamica Quaternaria 1984; 4:11-21.

Young J, Colella A. Calcarenous nannofossils from the Crati Basin. In: Colella A. (ed.), Fan Deltas-Excursion Guidebook. Università della Calabria, Cosenza, Italy. 79-96; 1988.

Kennedy, J., and Eberhart R.(1995): Particle swarm optimization. Neural Networks, 1995. Proceedings., IEEE International Conference on. Vol. 4. Perth, WA. IEEE, 1995.

Iovine GGR, Lollino P, Gariano SL, Terranova OG. Coupling limit equilibrium analyses and real-time monitoring to refine a landslide surveillance system in Calabria (southern Italy). Natural Hazards and Earth System Sciences 2010; 10:2341–2354.

Iverson RM. 2000. Landslide triggering by rain infiltration. Water Resources Research 36(7): 1897–1910

Jolliffe, I. T., & Stephenson, D. B. (Eds.). (2012). Forecast verification: a practitioner's guide in atmospheric science. University of Exeter, UK. John Wiley & Sons.

Lu, N., and J. Godt (2008), Infinite slope stability under steady unsaturated seepage conditions, Water Resour. Res., 44, W11404, doi:10.1029/2008WR006976.

Milledge, D. G., Bellugi, D., McKean, J. A., Densmore, A. L., & Dietrich, W. E. (2014). A multidimensional stability model for predicting shallow landslide size and shape across landscapes. *Journal of Geophysical Research: Earth Surface*, *119*(11), 2481-2504.

Montgomery, D. R., & Dietrich, W. E. (1994). A physically based model for the topographic control on shallow landsliding. Water resources research, 30(4), 1153-1171.

Murdoch, D. J., & Chow, E. D. (1996). A graphical display of large correlation matrices. *The American Statistician*, *50*(2), 178-180.

Naranjo, J.L., van Westen, C.J. and Soeters, R. (1994) Evaluating the use of training areas in bivariate statistical landslide hazard analysis: a case study in Colombia. ITC Journal, 3:292-300.

Pepe, M.S., 2003. The Statistical Evaluation of Medical Tests for Classification and Prediction. Oxford University Press, New York.

Park, N. W. (2011). Application of Dempster-Shafer theory of evidence to GIS-based landslide susceptibility analysis. *Environmental Earth Sciences*, *62*(2), 367-376.

Park, H. J., Lee, J. H., & Woo, I. (2013). Assessment of rainfall-induced shallow landslide susceptibility using a GIS-based probabilistic approach. Engineering Geology, 161, 1-15.

Provost, F., Fawcett, T., 2001. Robust classification for imprecise environments. Machine Learning 42 (3), 203–231.

Rosso, R., M. C. Rulli, and G. Vannucchi (2006), A physically based model for the hydrologic control on shallow landsliding, Water Resour. Res., 42, W06410, doi:10.1029/2005WR004369.

Sidle, R. C., & Ochiai, H. (2006). *Landslides: processes, prediction, and land use* (Vol. 18). Washington, DC 20009, USA. American Geophysical Union.

Simoni, S., Zanotti, F., Bertoldi, G., and Rigon, R. (2008): Modeling the probability of occurrence of shallow landslides and channelized debris flows using GEOtop-FS, Hydrol. Process., 22, 532{545,

Vezzani L. I terreni plio-pleistocenici del basso Crati (Cosenza). Atti dell’Accademia Gioenia di Scienze Naturali di Catania 6:28–84; 1968.

Vrugt, J. A., C. J. F. ter Braak, M. P. Clark, J. M. Hyman, and B. A. Robinson (2008), Treatment of input uncertainty in hydrologic modeling: Doing hydrology backward with Markov chain Monte Carlo simulation, Water Resour. Res., 44, W00B09, doi:10.1029/2007WR006720.

Table 1: Indices of goodness of fit for comparison between actual and predicted landslide.

Name	Definition	Range	Optimal value
Critical success index (CSI)	$\mathrm{CSI}=\frac{\mathrm{tp}}{\mathrm{tp+fp+fn}}$	[0 ,1]	1.0
Equitable success index (ESI)	$ESI=\frac{\mathrm{tp-R}}{\mathrm{tp+fp+fn-R}}$ $R=\frac{(tp+fn)\cdot(tp+fp)}{tp+fn+fp+tn}$	[-1/3,1]	1.0
Success Index (SI)	$\mathrm{SI}=\frac{1}{2}\cdot\left(\frac{tp}{tp+fn}+\frac{tn}{fp+tn}\right)$	[0 ,1]	1.0
Distance to perfect classification (D2PC)	$D2PC=\sqrt{(1-TPR)^2+FPR^2}$ $\mathrm{TPR}=\frac{\mathrm{tp}}{\mathrm{tp+fn}}$ $\mathrm{FPR}=\frac{\mathrm{fp}}{\mathrm{fp+tn}}$	[0,1]	0.0
Average Index (AI)	$AI=\frac{1}{4}\left(\frac{tp}{tp+fn}+\frac{tp}{tp+fp}+\frac{tn}{fp+tn}+\frac{tn}{fn+tn}\right)$	[0,1]	1.0
True skill statistic (TSS)	$TSS=\frac{(tp\cdot tn)-(fp\cdot fn)}{(tp+fn)\cdot(fp+tn)}$	[-1,1]	1.0
Heidke skill score (HSS)	$HSS=\frac{2\cdot(tp\cdot tn)-(fp\cdot fn)}{(tp+fn)\cdot(fn+tn)+(tp+fp)\cdot(fp+tn)}$	[-∞, 1]	1.0
Accuracy (ACC)	$ACC=\frac{(\mathrm{tp}+\mathrm{tn})}{(\mathrm{tp}+\mathrm{fn}+\mathrm{fp}+\mathrm{tn})}$	[0,1]	1.0

Table 2: Optimised models' parameters values

Model Parameters	**Constant Value**	**Range value**
Soil Depth [m]	-	[0.8; 5.0]
Transmissivity [m2/d]	-	[10; 150]
Soil/water density ratio	-	[1.8; 2.8]
Friction Angle [°]	-	[11; 40]
Rainfall [mm/d]	-	[50; 300]
Soil Cohesion [kPa]	-	[0; 50]
Degree Of Saturation [-]	0.5	-
Soil Porosity [-]	0.5	-
Rainfall Duration [d]	-	[0.1; 3.0]

Table 3: Optimal parameter sets output of the optimization procedure of each GOF indices in turn. Results are presented for each model (M1, M2 and M3).

Model: M1								
Optimised Index	AI	HSS	TSS	D2PC	SI	ESI	CSI	ACC
Soil Depth [m]	1.32	1.85	1.44	2.80	1.36	2.62	2.42	2.01
Transmissivity [m2/d]	140.24	146.31	142.68	137.10	147.69	144.66	136.73	74.74
Soil/water density ratio [-]	2.61	2.56	2.77	2.71	2.78	2.79	2.63	2.72
Friction Angle [°]	24.20	32.40	22.50	23.10	22.40	29.50	29.50	38.30
Rainfall [mm/d]	85.38	53.30	71.36	50.00	52.69	69.19	61.35	141.80

Model: M2								
Optimised Index	AI	HSS	TSS	D2PC	SI	ESI	CSI	ACC
Transmissivity [m2/d]	65.43	33.22	80.45	38.22	84.54	33.24	10.70	55.76
Cohesion [kPa]	25.17	49.63	49.42	16.94	30.01	41.24	44.58	46.85
Friction Angle [°]	29.51	38.38	20.01	32.30	24.57	33.78	35.68	34.96
Rainfall [mm/d]	236.14	293.44	270.42	153.61	294.70	298.44	95.35	299.01
Soil/water density ratio [-]	2.11	2.40	2.06	2.44	2.77	2.17	2.55	2.19
Soil Depth [m]	2.35	1.68	2.38	2.44	2.74	1.12	1.37	1.12

Model: M3								
Optimised Index	AI	HSS	TSS	D2PC	SI	ESI	CSI	ACC
Transmissivity [m2/d]	30.95	26.55	47.03	36.31	57.28	25.84	31.60	48.71
Cohesion [kPa]	36.88	44.33	28.51	31.60	45.46	41.80	32.05	37.09
Friction Angle [°]	19.55	36.44	27.80	29.70	21.46	33.27	36.47	38.50
Rainfall [mm/d]	248.77	230.08	258.82	201.71	299.90	291.32	273.03	193.02
Soil/water density ratio [-]	2.40	2.57	2.08	2.80	2.65	2.63	2.61	2.44
Soil Depth [m]	1.84	1.42	2.23	2.92	2.85	1.17	1.13	1.15
Rainfall Duration [d]	0.12	1.78	1.24	1.96	1.24	0.39	1.30	1.98

Table 4: Results in term of true-positive rate (TPR) and false-positive rate (FPR), for each model (M1, M2 and M3), for each optimised GOF index and for both calibration (CAL) and verification (VAL) dataset. In bold are shown the rows for which the condition FPR<0.4 and TPR>0.7 is verified.

		MODEL: M1		MODEL: M2		MODEL: M3	
Period	Optim. Index	FPR	TPR	FPR	TPR	FPR	TPR
CAL	ACC	0.04	0.12	0.03	0.12	0.03	0.13
CAL	**AI**	**0.29**	**0.70**	**0.35**	**0.79**	**0.38**	**0.82**
CAL	CSI	0.17	0.48	0.10	0.36	0.09	0.32
CAL	**D2PC**	**0.32**	**0.72**	**0.32**	**0.76**	**0.32**	**0.75**
CAL	ESI	0.17	0.48	0.43	0.82	0.09	0.36
CAL	HSS	0.12	0.35	0.09	0.35	0.09	0.35
CAL	**SI**	**0.34**	**0.74**	**0.39**	**0.85**	**0.39**	**0.86**
CAL	**TSS**	**0.34**	**0.73**	**0.39**	**0.83**	**0.37**	**0.82**
VAL	ACC	0.05	0.12	0.03	0.12	0.03	0.10
VAL	AI	0.26	0.56	0.31	0.69	**0.34**	**0.72**
VAL	CSI	0.17	0.39	0.09	0.31	0.08	0.29
VAL	D2PC	0.29	0.59	0.28	0.67	0.28	0.66
VAL	ESI	0.17	0.39	0.41	0.76	0.09	0.30
VAL	HSS	0.12	0.30	0.09	0.30	0.09	0.30
VAL	SI	0.30	0.61	**0.37**	**0.75**	**0.39**	**0.76**
VAL	TSS	0.30	0.62	**0.35**	**0.74**	**0.34**	**0.71**

Figure 1: Integration of the Landslide susceptibility analysis system in NweAge-JGrass hydrological model.

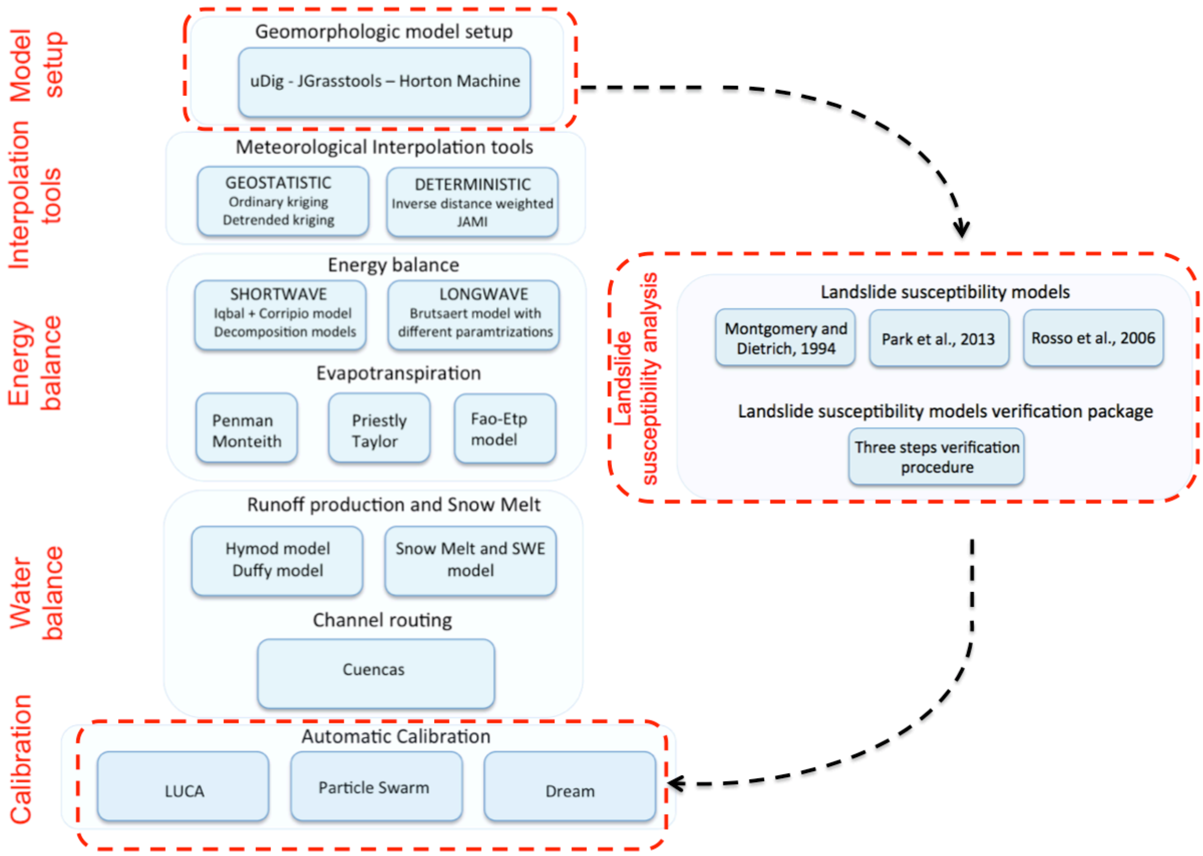
Model setup
Geomorphologic model setup
uDig - JGrasstools – Horton Machine
Interpolation tools
Meteorological Interpolation tools
GEOSTATISTIC
Ordinary kriging
Detrended kriging
DETERMINISTIC
Inverse distance weighted
JAMI
Energy balance
Energy balance
SHORTWAVE
Iqbal + Corripio model
Decomposition models
LONGWAVE
Brutsaert model with
different paramtrizations
Evapotranspiration
Penman Monteith
Priestly Taylor
Fao-Etp model
Water balance
Runoff production and Snow Melt
Hymod model
Duffy model
Snow Melt and SWE model
Channel routing
Cuencas
Calibration
Automatic Calibration
LUCA
Particle Swarm
Dream
Landslide susceptibility analysis
Landslide susceptibility models
Montgomery and Dietrich, 1994
Park et al., 2013
Rosso et al., 2006
Landslide susceptibility models verification package
Three steps verification procedure

Figure 2: Test site. A) Digital elevation model (DEM) [m], B) slope [-] expressed as tangent of the angle, C) total contributing area (TCA) expressed as number of draining cells and D) Map of actual landslides.

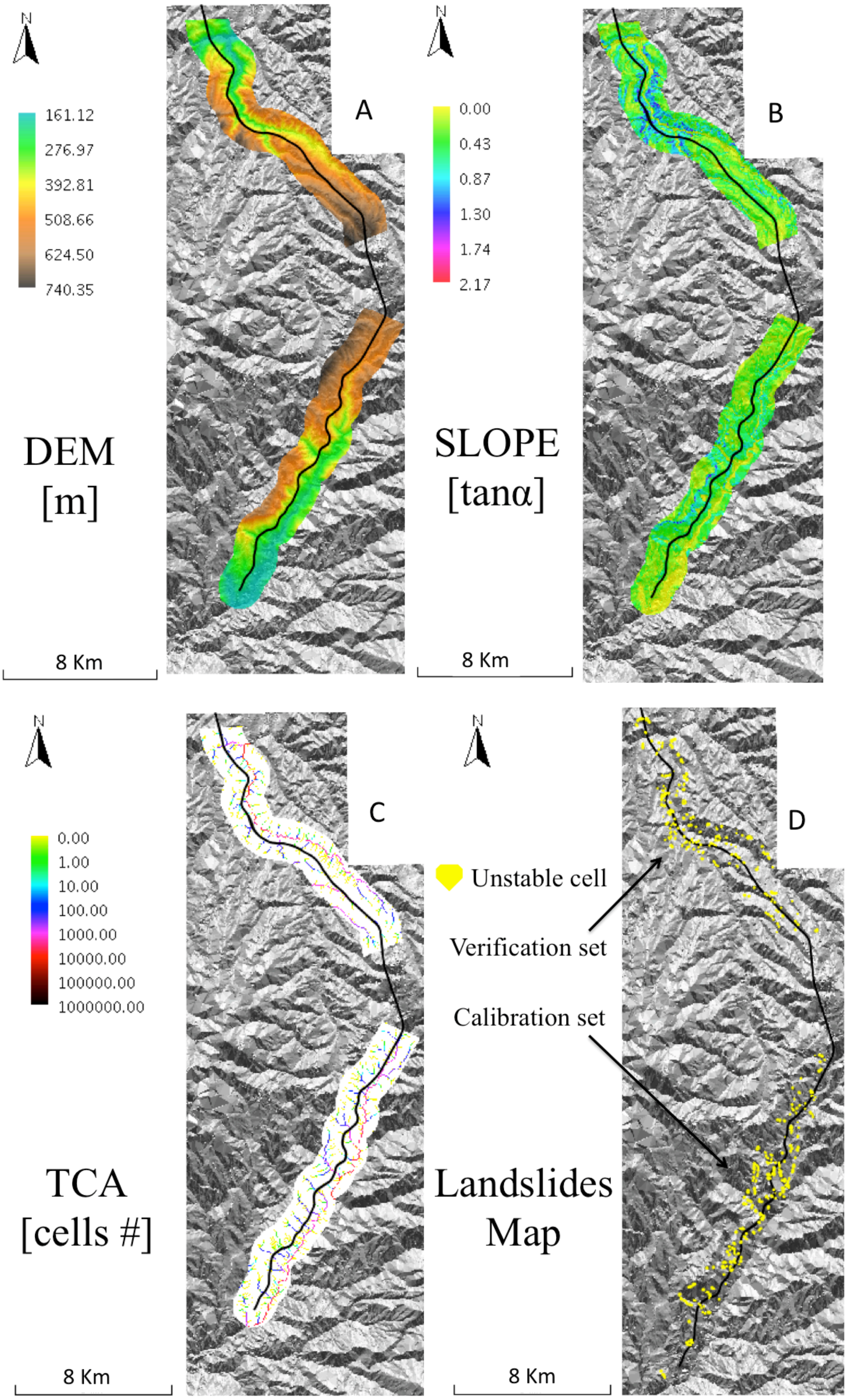
A
161.12
276.97
392.81
508.66
624.50
740.35
DEM
[m]
8 Km
B
0.00
0.43
0.87
1.30
1.74
2.17
SLOPE
[tanα]
8 Km
C
0.00
1.00
10.00
100.00
1000.00
10000.00
100000.00
1000000.00
TCA
[cells #]
8 Km
D
Unstable cell
Verification set
Calibration set
Landslides
Map
8 Km

Figure 3: Models' performances results in the ROC plane for M1, M2 and M3. Only GOF indices whose optimization provides FPR<0.4 and TPR>0.7 were reported.

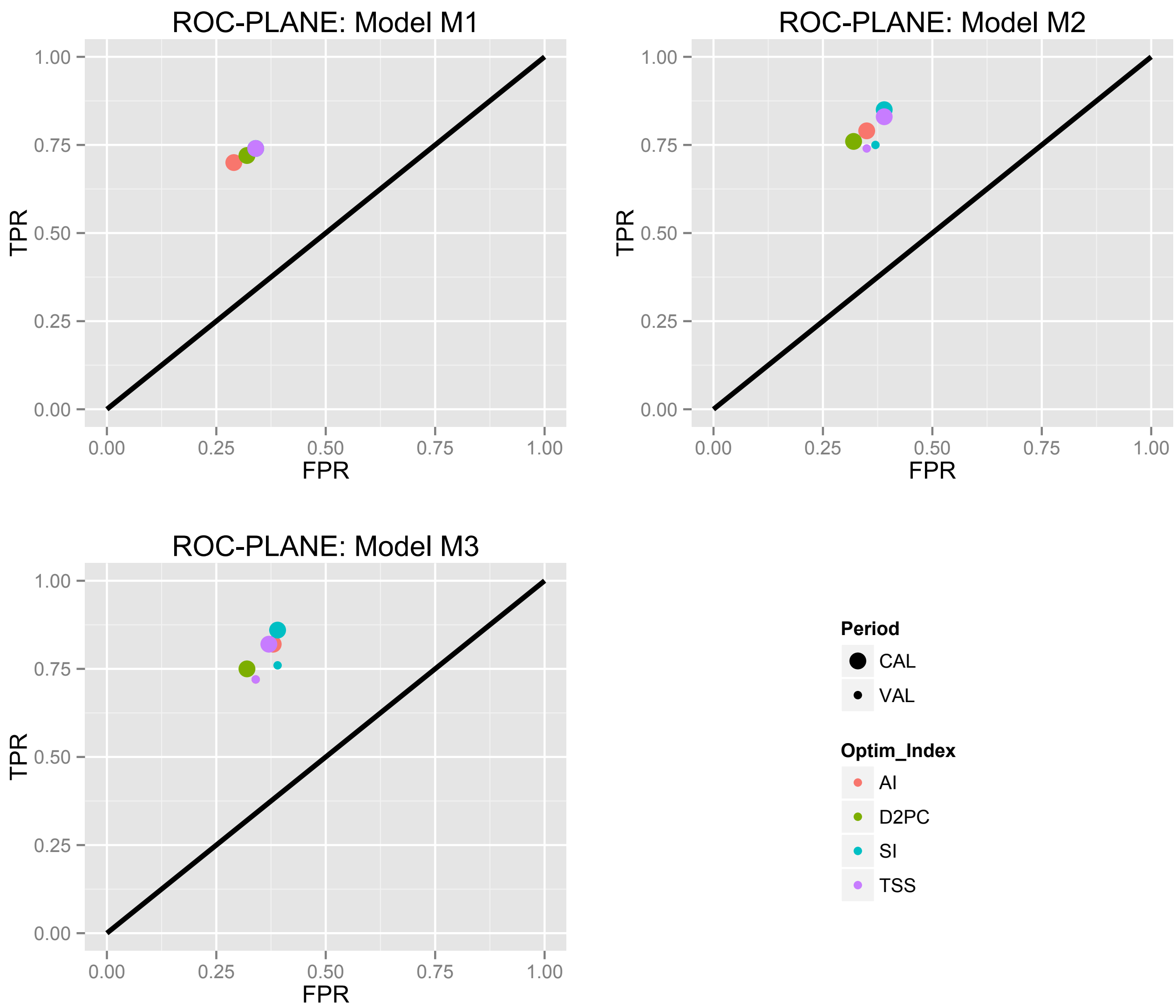

Figure 4: Correlation plot between models' performance (MP) vector computed by optimizing all GOF indices in turn. Results are reported for each model: M1, M2 and M3.

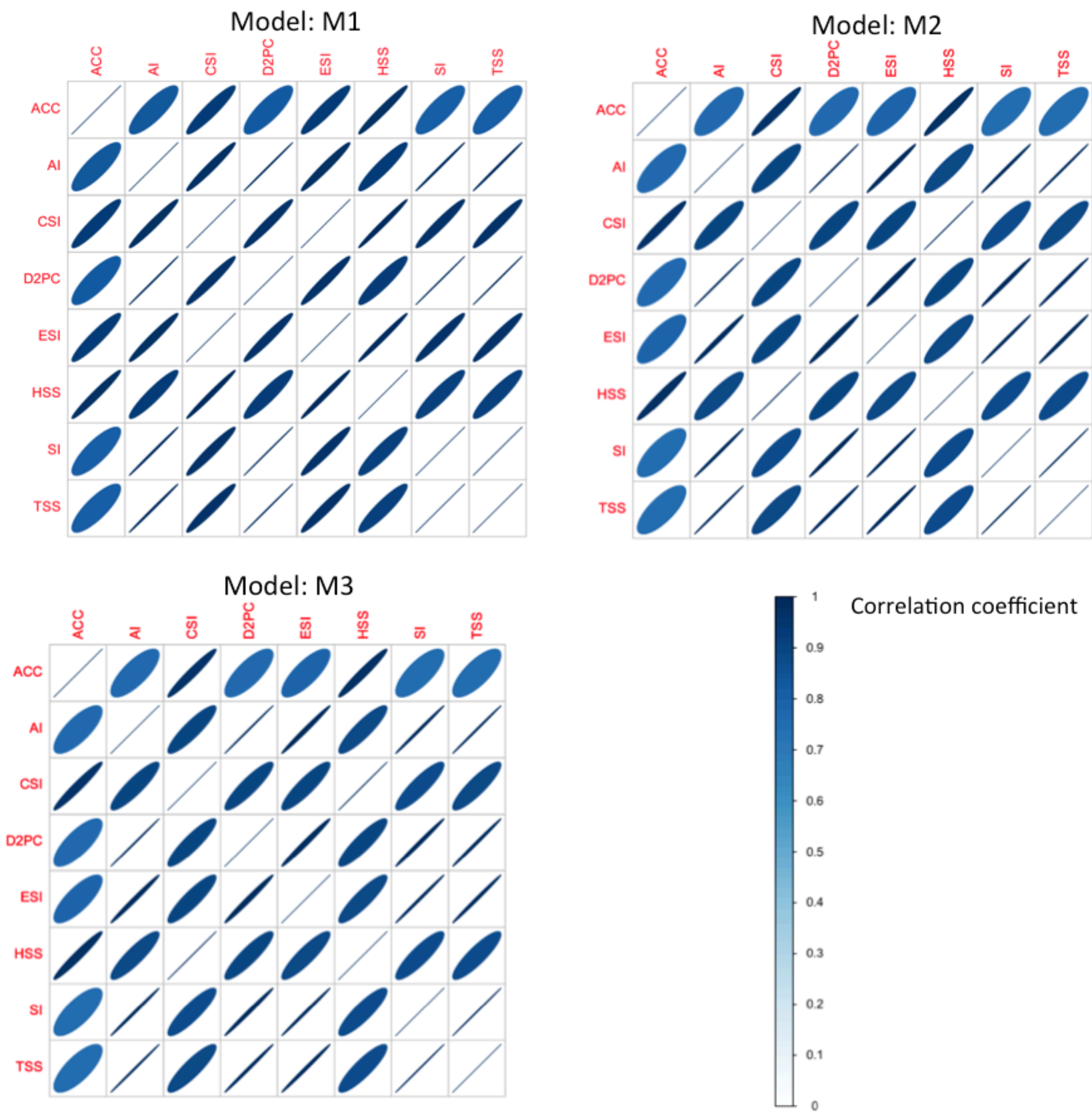

Figure 5: Model M2 parameters sensitivity analysis.

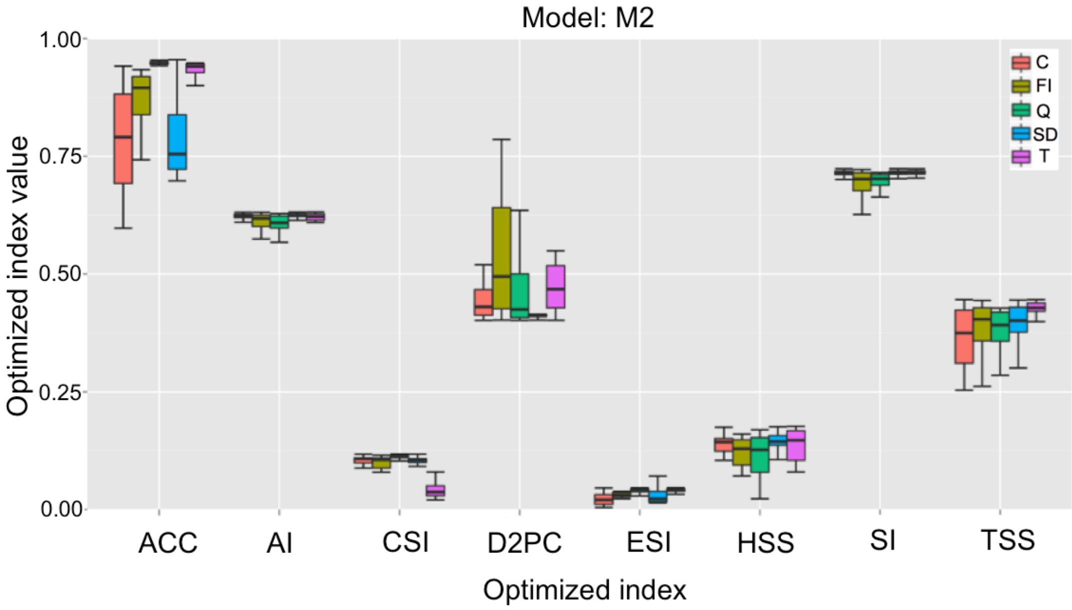

Figure 6: Model M3 parameters sensitivity analysis.

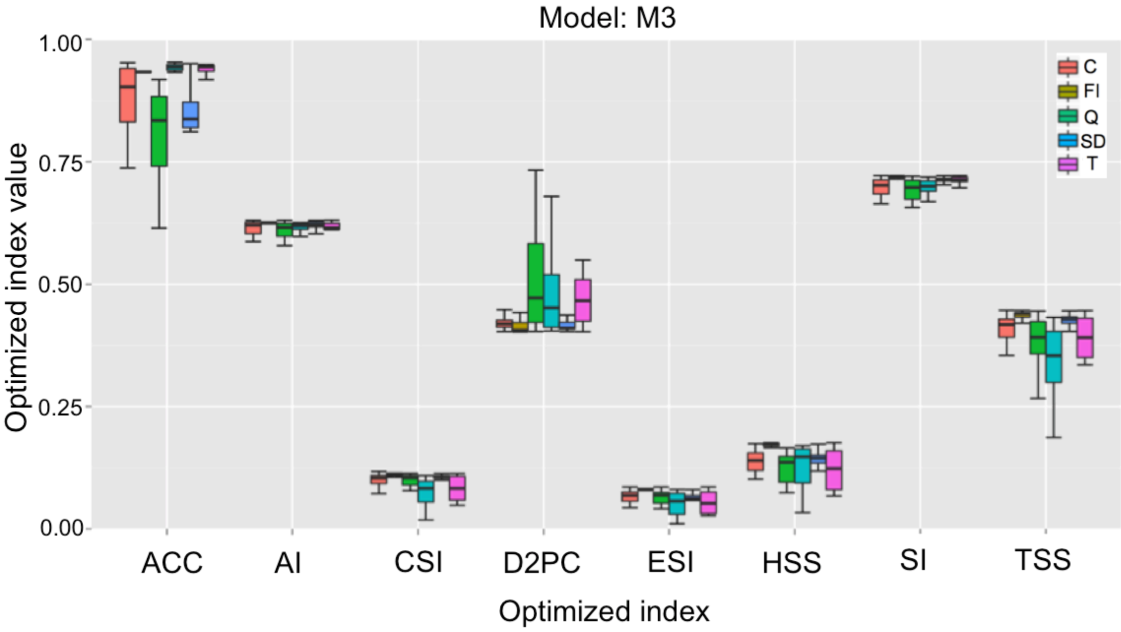

Figure 7: Landslide susceptibility maps using model M3 and parameter set obtained by optimising D2PC.

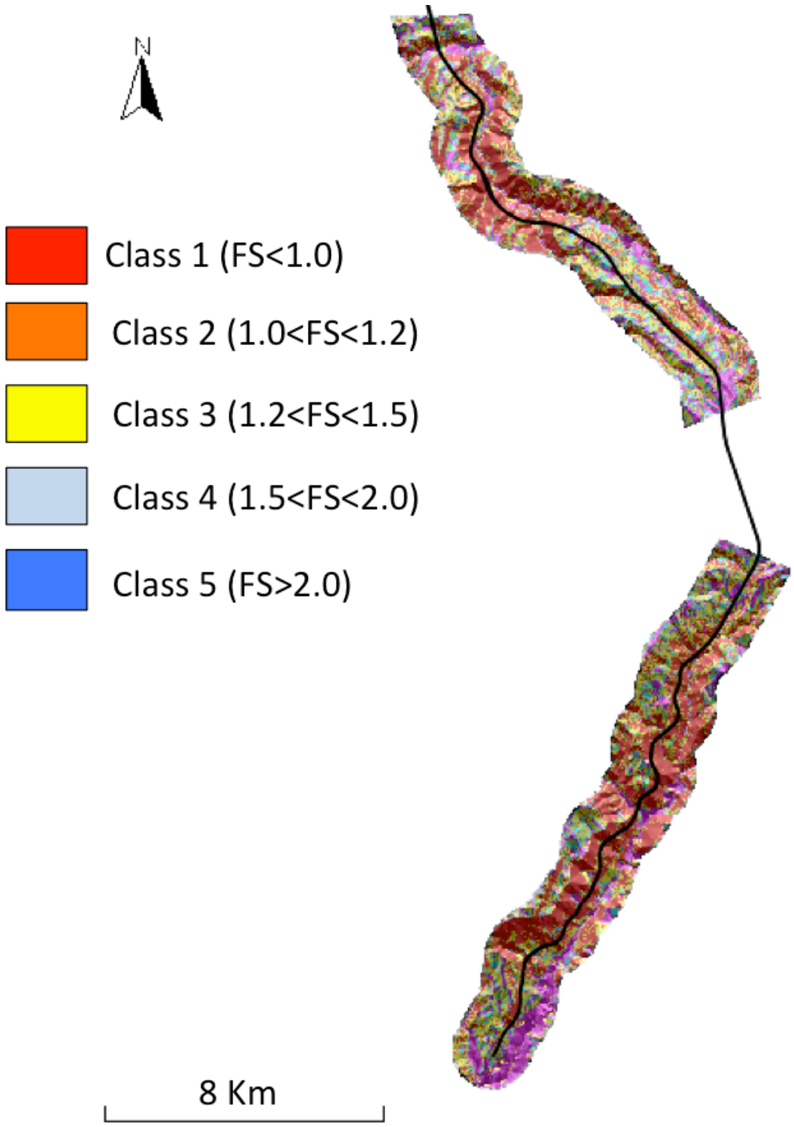

Appendix 1

1.2 Critical success index (CSI)

CSI, eq. (2), is the number of correct detected lindslide pixels (tp), divided by the sum of tp, fn and fp. CSI is also named threat score. It range between 0 and 1 and its best value is 1. It penalizes both fn and fp.

$$\mathrm{CSI}=\frac{\mathrm{tp}}{\mathrm{tp+fp+fn}} \quad (2)$$

1.3 Equitable success index (ESI)

ESI, eq. (3), contrarily to CSI, is able to take into account the true positives associated with random chance (R). ESI ranges between -1/3 and 1. Value 1 indicates perfect score.

$$E\mathrm{SI}=\frac{\mathrm{tp-R}}{\mathrm{tp+fp+fn-R}} \quad 3)$$

$$R=\frac{(tp+fn)\cdot(tp+fp)}{tp+fn+fp+tn} \quad (4)$$

1.4 Success index (SI)

SI, eq.(5), equally weight True positive rate (eq. 6) and specificity defined as 1 minus false positive rate (FPR), eq. (7). SI varies between 0 and 1 and its best value is 1. SI is also named modified success rate.

$$\mathrm{SI}=\frac{1}{2}\cdot\left(\frac{tp}{tp+fn}+\frac{tn}{fp+tn}\right)=\frac{1}{2}\cdot\left(\mathrm{TPR}+\mathrm{specificity}\right) \quad (5)$$

$$\mathrm{TPR}=\frac{\mathrm{tp}}{\mathrm{tp+fn}} \quad (6) \qquad \mathrm{FPR}=\frac{\mathrm{fp}}{\mathrm{fp+tn}} \quad (7)$$

1.5 Distance to perfect classification (D2PC)

D2PC is defined in eq. (8). It measures the distance, in the plane FPR-TPR between an ideal perfect point of coordinates (0,1) and the point of the tested model (FPR,TPR). D2PC ranges in 0-1 and its best value are 0.

$$D2PC=\sqrt{\left(1-TPR\right)^{2}+FPR^{2}} \quad (8)$$

1.6 Average Index (AI)

AI, eq. (9), is the average value between four different indices: i) TPR, ii) Precision, iii) the ratio between successfully predicted stable pixels (tn) and the total number of actual stable pixels (fp+tn) and iv) the ratio between successfully predicted stable pixels (tn) and the number of simulated stable cells (fn+tn).

$$AI=\frac{1}{4}\left(\frac{tp}{tp+fn}+\frac{tp}{tp+fp}+\frac{tn}{fp+tn}+\frac{tn}{fn+tn}\right) \quad (9)$$

1.7 Heidke skill score (HSS)

The fundamental idea of a generic skill score measure is to quantify the model performance respect to set of control or reference model. Fixed a measure of model accuracy M_a, the skill score formulation is expressed in eq. (10):

$$SS=\frac{M_a - M_c}{M_{opt} - M_c} \quad (10)$$

where M_c is the control or reference model accuracy and M_{opt} is the perfect model accuracy.

SS assumes positive and negative value, if the tested model is perfect $M_a = M_{opt}$ and SS=1, if the tested model is equal to the control model than $M_a = M_c$ and SS=0.

The marginal probability of a predicted unstable pixel is (tp+fp)/n where n is the total number of pixels n=tp+fn+fp+tn. The marginal probability of a landslided unstable pixel is (tp+fn)/n.

The probability of a correct yes forecast by chance is: P1= (tp+fp) (tp+fn)/n^2. The probability of a correct no forecast by chance is: P2= (tn+fp) (tn+fn)/n^2.

In the HSS, eq. (11), the control model is a model that forecast by chance: M_c = P1+ P2, the measure of accuracy is the Accuracy (ACC) defined in eq. (12), and the M_{opt}=1.

$$HSS=\frac{2\cdot(tp\cdot tn)-(fp\cdot fn)}{(tp+fn)\cdot(fn+tn)+(tp+fp)\cdot(fp+tn)} \quad (11)$$

$$\mathrm{ACC}=\frac{\mathrm{tp+tn}}{\mathrm{tp+fn+fp+tn}} \quad (12)$$

The range of the HSS is -∞ to 1. Negative values indicate that the model provides no better results of a random model, 0 means no model skill, and a perfect model obtains a HSS of 1. HSS is also named as Cohen's kappa.

1.8 True Skill Statistic (TSS)

TSS, eq. (13), is the difference between the hit rate and the false alarm rate. It is also named Hanssen & Kuipper's Skill Score and Pierce's Skill Score. It ranges between -1 and 1 and its best value is 1. TSS equal -1 indicates that the model provides no better results of a random model. A TSS equal 0 indicates an indiscriminate model.

TSS measures the ability of the model to distinguish between landslided and non-landslided pixels. If the number of tn is large the false alarm value is relatively overwhelmed. If tn is large, as happens in landslides maps, FPR tends to zero and TSS tends to TPR. A problem of TSS is that it treats the hit rate and the false alarm rate equally, irrespective of their likely differing consequences.

$$TSS=\frac{(tp \cdot tn)-(fp \cdot fn)}{(tp+fn)\cdot(fp+tn)}=TPR-FPR \quad (13)$$

TSS is similar to Heidke, except the constraint on the reference forecasts is that they are constrained to be unbiased.

Appendix 2

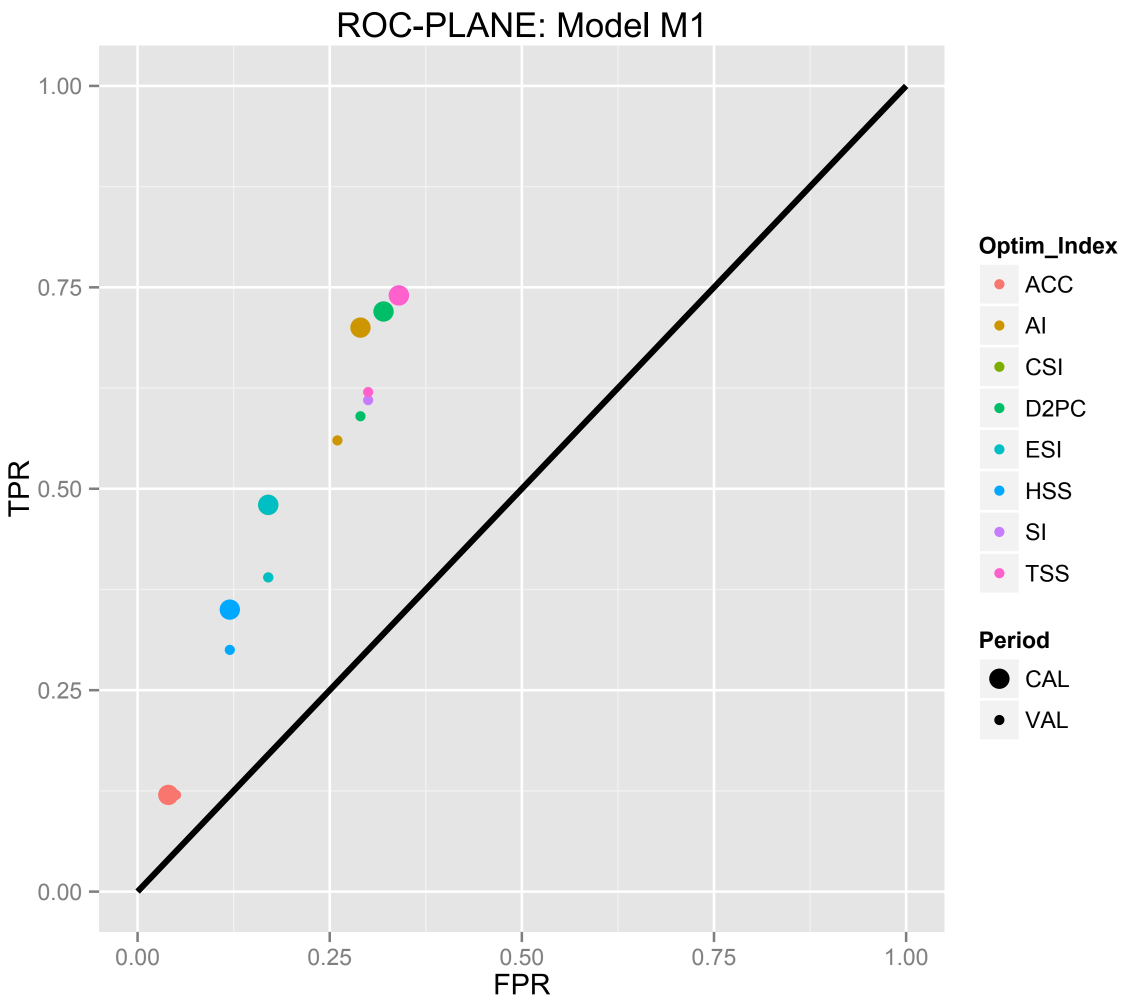

Figure A2-1: Models' performances results in the ROC plane for M1.

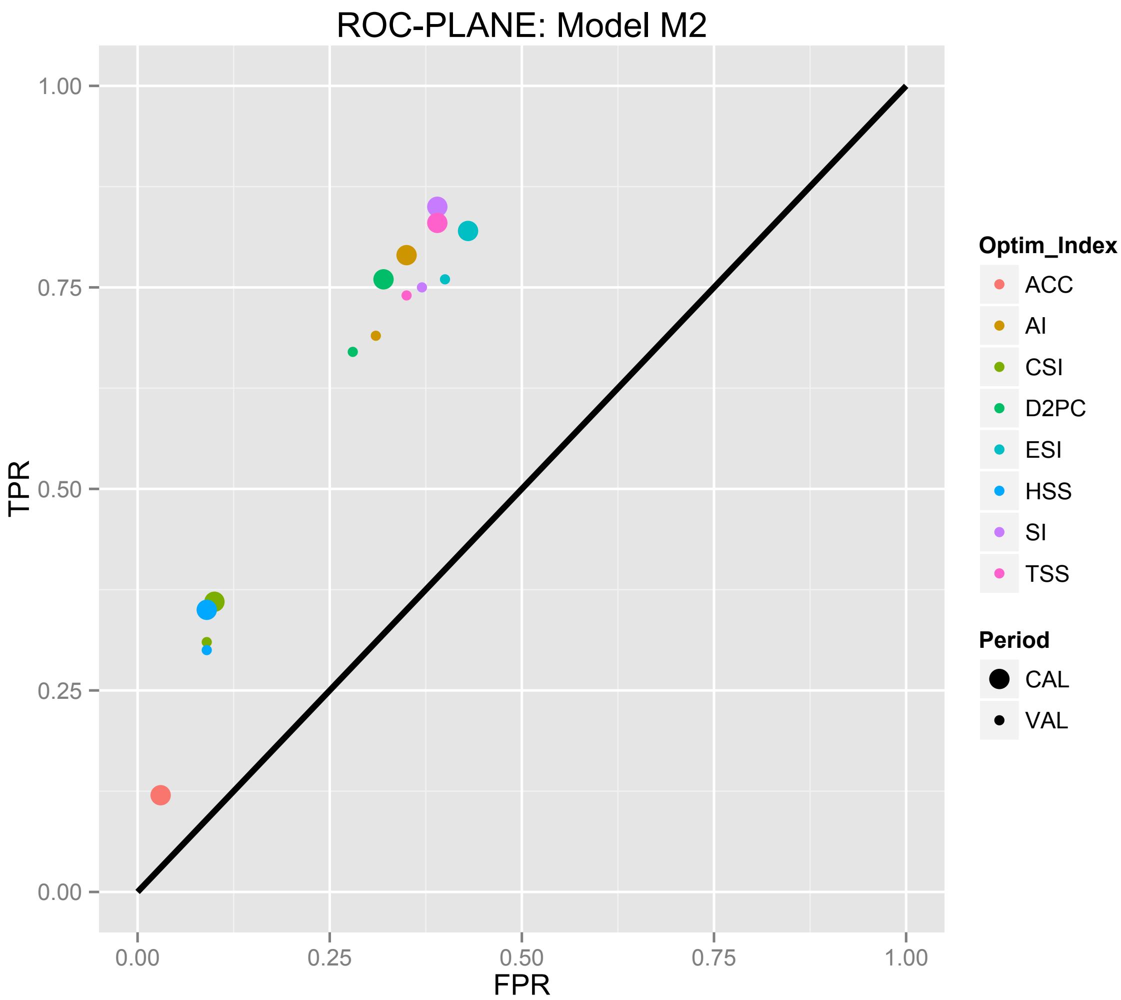

Figure A2-2: Models' performances results in the ROC plane for M2.

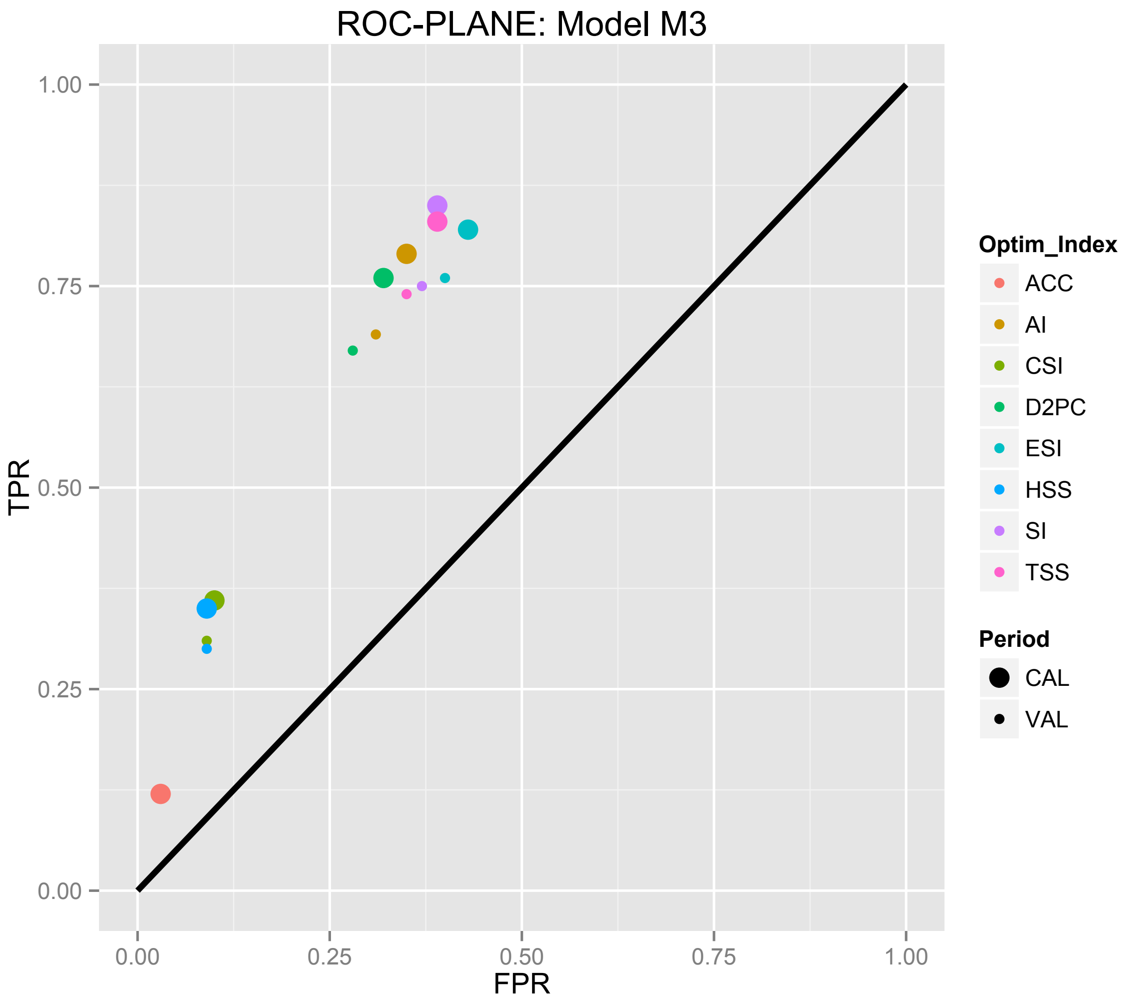

Figure A2-3: Models' performances results in the ROC plane for M3.